Composites Part B 254 (2023) 110576

Contents lists available at ScienceDirect

Composites Part B

journal homepage: www.elsevier.com/locate/compositesb

Non-conventional failures caused by the edge effect in cross-ply laminates made of ultra-thin plies

S. Sánchez-Carmona, A. Barroso *, V. Mantič, E. Correa, F. París

Grupo de Elasticidad y Resistencia de Materiales, Departamento de Mecánica de Medios Continuos y Teoría de Estructuras, Escuela Técnica Superior de Ingeniería, Universidad de Sevilla, Camino de los Descubrimientos, 41092, Sevilla, Spain

ARTICLE INFO

Handling Editor: Prof. Ole Thomsen

Keywords:
Edge-effect
Ultra-thin plies
Longitudinal damage
Stress singularity
Composite materials

ABSTRACT

In a fatigue testing programme of carbon/epoxy cross-ply laminates made of ultra-thin plies, non-conventional failures are observed. These non-conventional failures consist in longitudinal cracks in the 90° layer parallel to the loading direction instead of the conventional transverse cracks in the 90° layer perpendicular to the load direction. A potential reason for this failure is the presence of a normal stress in the thickness direction. Classical Lamination Theory predicts zero values for this stress component under longitudinal loading, but the presence of a free-edge alters the stress state. The so-called "edge-effect" has been widely studied in the past, but the presence of ultra-thin plies introduces new lower limits of the thickness of the 90° layer. Additionally, the presence of a stress singularity, in the bimaterial corner generated by the 0° and 90° plies, is also investigated to check its influence on the stress state due to the low thickness values of the 90° layer. A slight geometrical modification is conceived to remove the stress singularity, isolating its effect from the pure edge effect. Numerical simulations of the stress alteration in the free edge of the samples, due to mechanical and thermal loading, are carried out, and stress distributions are numerically computed, depending on the 90° layer thickness. Detailed failure inspection by 3D tomography is also done to assess the through-the-width propagation of the non-conventional failures from the free edge. Numerical predictions and experimental 3D X-ray inspections seem to corroborate that the edge effect is responsible for these non-conventional failures.

1. Introduction

During a fatigue testing programme with cross-ply laminates manufactured with unidirectional carbon-fibre/epoxy ultra-thin plies, non-conventional failures were observed (Sánchez-Carmona et al. [1]). What is usually expected in these cross-ply laminates under static (tension) loading, or fatigue (tension-tension) loading, is a first transverse failure in the inner 90° layer. With different cross-ply configurations, keeping the 0° plies group with a constant thickness, and gradually decreasing the 90° layer thickness, failure patterns clearly showed a different behaviour, from a transverse crack pattern (Fig. 1a, perpendicular to the longitudinal load direction) to a longitudinal crack pattern (Fig. 1b, parallel to the longitudinal load direction).

The fatigue testing programme was oriented to assess if the so-called "scale effect", observed in static testing (Parvizi et al. [2], Flaggs & Kural [3], or more recently by García et al. [4], París et al. [5]), for the apparent transverse strength increment in the 90° layer, was also observed under fatigue loading. Therefore, during the fatigue loading, a detailed inspection of failure onset and progression was carried out. The inspection was performed at the edges of the samples by means of replica-based crack inspection (i.e. in-situ observation, due to the fact that the inspection is carried out without the need to disassemble the sample from the fatigue machine) and/or optical microscopy (i.e. ex-situ observation).

The crack pattern previously described for laminates with ultra-thin plies in the 90° layer was systematically observed as the 90° layer thickness was decreasing, the present work being an attempt to understand this non-conventional failure mechanism. Cross-ply laminates used in the present work include 4 outer 0° plies of 150 g/m^2 and central 90° plies with the following grammages and ply thicknesses, respectively: 3 × 150 g/m^2 (0.485 mm), 100 g/m^2 (0.1 mm), 50 g/m^2 (0.065 mm) and 30 g/m^2 (0.06 mm). These laminates will be referred to as "450", "100", "50" and "30" respectively.

The alteration of the stress state at a free edge (the so-called edge-effect) is explored in the present work as the main reason responsible for the change of the failure pattern. Nevertheless, the bimaterial corner

* Corresponding author.
E-mail address: abc@us.es (A. Barroso).

https://doi.org/10.1016/j.compositesb.2023.110576
Received 11 November 2022; Received in revised form 22 December 2022; Accepted 27 January 2023
Available online 1 February 2023
1359-8368/© 2023 The Author(s). Published by Elsevier Ltd. This is an open access article under the CC BY-NC-ND license (http://creativecommons.org/licenses/by-nc-nd/4.0/).

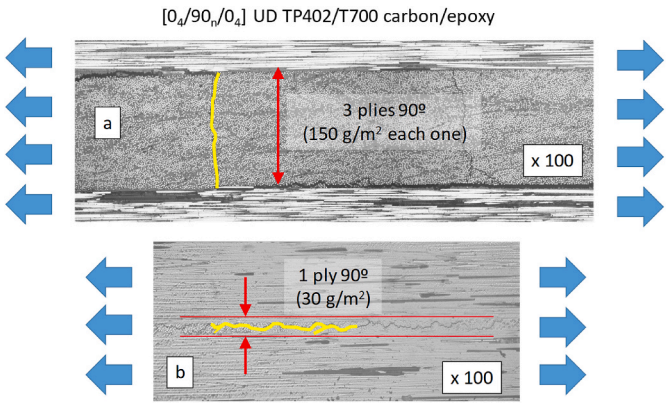

Fig. 1. Failure patterns in $[0_4/90_n/0_4]$ UD TP402/T700 carbon/epoxy laminates using a) conventional "thick" 90° plies, b) ultra-thin 90° ply.

configuration appearing at any point of the intersection line of the 0°/90° interface and the free edge, generates a singularity stress field due to the abrupt change in material properties (abrupt change in fibre orientation indeed). Although it is accepted that unbounded stresses cannot be materialized at these points, these stress intensifications have shown, with experimental evidences, to influence premature failure onset (Barroso et al. [6]). This local alteration of the stress state might play a relevant role in the case of laminates with ultra-thin plies if it affects a significant part of the 90° ply thickness.

To separate the effect of the stress singularity and the free edge, a slight change in the local geometry of the corner has been carried out in the numerical models. The stress singularities depend on the material properties, on the local geometry and on the local boundary conditions. The best way to change, and consequently remove, the stress singularity is by means of a slight change of the local geometry of the corner, which simply consists in modifying one of the wedge angles of one of the plies. This slight geometrical modification does not significantly alter the edge effect, and changes significantly the values of the stress singularities at the corner. This aspect will be detailed later in Section 3.

With the above-mentioned ideas in mind, in the present paper a fourfold way has been followed to present a plausible explanation for the observed non-conventional failures in the cross-ply laminates made of ultra-thin 90° plies.

1) Edge-effect is revisited (Section 2), keeping in mind that ultra-thin plies play an important role in the stress state alteration. Classical, as well as more recent works, have been re-read, without the intention to make a comprehensive review, but to clearly understand the qualitative and quantitative influence of the edge-effect on the stress state.
2) Semi-analytical analyses, as well as numerical simulations, are carried out (Section 3) to check the extent of the singular stress field. Although some previous works have taken this effect into account, the novelty of using ultra-thin plies, makes this (in some cases very local) alteration of the stress field to play a significant role in the failure onset. This part of the work has been possible thanks to the previous experience and the existence of a code, developed by the authors [17,18], to evaluate stress singularities in multimaterial corners with anisotropic materials. A slight modification of the local geometry of the corner is carried out numerically, to remove the stress singularity field, isolating the edge-effect.
3) Detailed numerical simulations are performed (Section 4) to check the alteration of the stress field at the free edge, both due to the mechanical effect and also due to the residual thermal stress field. The mismatch of the mechanical, and thermal, properties between the different layers leads to the appearance of the edge effect in both types of loading. Also, some experiments with non-symmetric laminates are carried out in the present work to evaluate the relaxation with time of the residual thermal stresses.
4) Using 3D computed tomography (ZEISS Xradia 620 Versa), detailed 3D images of the non-conventional failures at the free edge have been obtained at the micro-scale level (Section 5). These experimental observations give the necessary evidence about the through-the-width progression of these non-conventional failures.

2. Edge effect

The so-called "edge effect", although originally considered only for interlaminar shear stresses in angle-ply laminates of finite width, can be understood (in the framework of composite laminates) as the alteration of the stress state when approaching a free edge.

Pipes & Pagano [7] is a classical reference where finite-width angle-ply laminates $[+\alpha/-\alpha/-\alpha/+\alpha]$ are subjected to tension. Interlaminar stresses along the interfaces between plies were obtained numerically, using finite-differences. Alterations in the predicted solution from Classical Lamination Theory (valid for infinite width problems), which are needed to fulfil the boundary conditions, were observed at the free edge and affecting a characteristic length equal to the laminate thickness in the width direction.

Although it is going to be treated separately (in Section 3), in Pipes & Pagano [7] it was also explicitly mentioned the presence of a singularity at the free edge, "*Finally, we have seen strong evidence of a singularity in the interlaminar shear stress at the intersection of the interface and free-edge.*", as potential location for delamination under fatigue loading.

Notwithstanding the phenomenon does not change from a qualitative point of view, Pipes & Pagano [7] did not include cross-ply laminate configurations. Some years later, Pagano and Soni [8] presented a comprehensive review of the free-edge effect in composite laminates, which is an excellent summary of this particular phenomenon.

Closed form solutions for the interlaminar stresses have also been addressed in literature. Kassapoglou & Lagace [9] obtained solutions for angle-ply and cross-ply laminates using the Force Balance Method and the Principle of Minimum Complementary Energy, while Becker [10] obtained the solution for cross-ply laminates using a higher-order plate theory.

Pagano et al. [11] presented the analysis of the edge-effect, now in cross-ply laminates, including mechanical as well as thermal loading. The influence of the 90° layer thickness, using conventional plies (0.125 mm thickness), on the transverse cracking of the sample was investigated, but no reference to longitudinal cracking inside the 90° layer was mentioned in the work. This non-conventional failure pattern, which has motivated the present work, has appeared when ultra-thin plies are involved, which were not taken into consideration in the mentioned work [11].

Lorriot et al. [12] investigated free-edge delaminations in different configurations ($[\pm 15_n]_S$, $[\pm 20_n]_S$, $[\pm 30_n]_S$ …) activating mode III at the interface, as well as other stacking sequences, including a central 90° layer to induce potential longitudinal failures by normal stresses in the thickness direction. The tests were conducted using conventional ply thickness (0.125 mm), and without an explicit cross-ply configuration.

An excellent comprehensive review of the edge effect in composite laminates can be found in two papers by Mittelstedt & Becker (2007) [13] and Mittelstedt et al. (2022) [14]. The first one covering the research carried out since the pioneering works in 1967–2005, and the second one, from 2005 to 2022.

Fig. 2 shows the global scheme of the problem (Fig. 2a), the section of interest (Fig. 2b) and the final analyzed problem, making use of the symmetry of the problem (Fig. 2c), where the y axis corresponds to the thickness of the laminate, and the z axis is the direction of the applied load.

Assuming that the normal stress in the thickness direction is a natural candidate to originate the observed longitudinal cracks inside the 90° layer, the understanding of the edge effect for the cross-ply

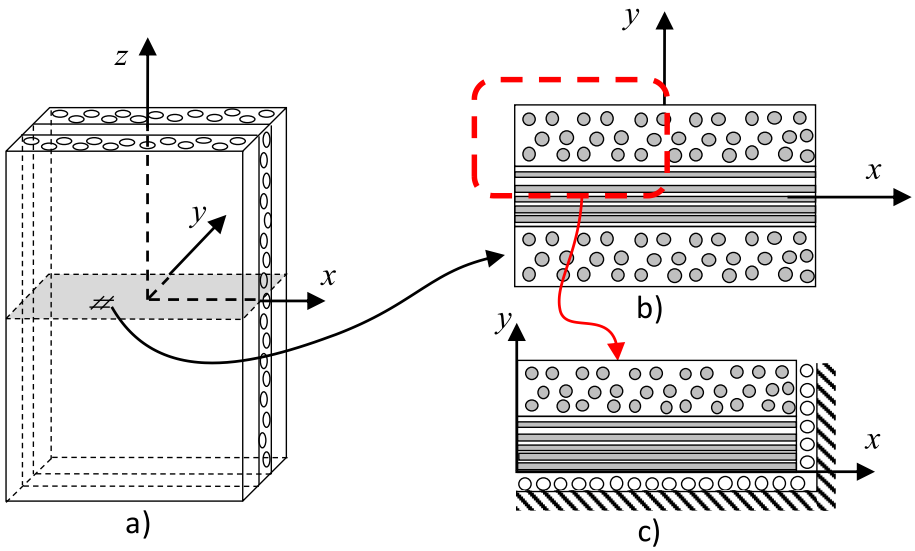

Fig. 2. Scheme of the problem under analysis.

configuration is necessary. Notice that other potential transverse failure initiation proposals, such as cavitation (see, for example [24]), have not been explored in the present work. Also notice that no failure has been observed in the 0/90 interface, which suggests that due to the complexity of the geometry at the microscale level where the two plies meet, the corresponding interface strength is higher than the bulk transverse strength of the 90° layer. The role of the transverse strength (Y_t) on the failure of the 90° layer with different ply thicknesses is

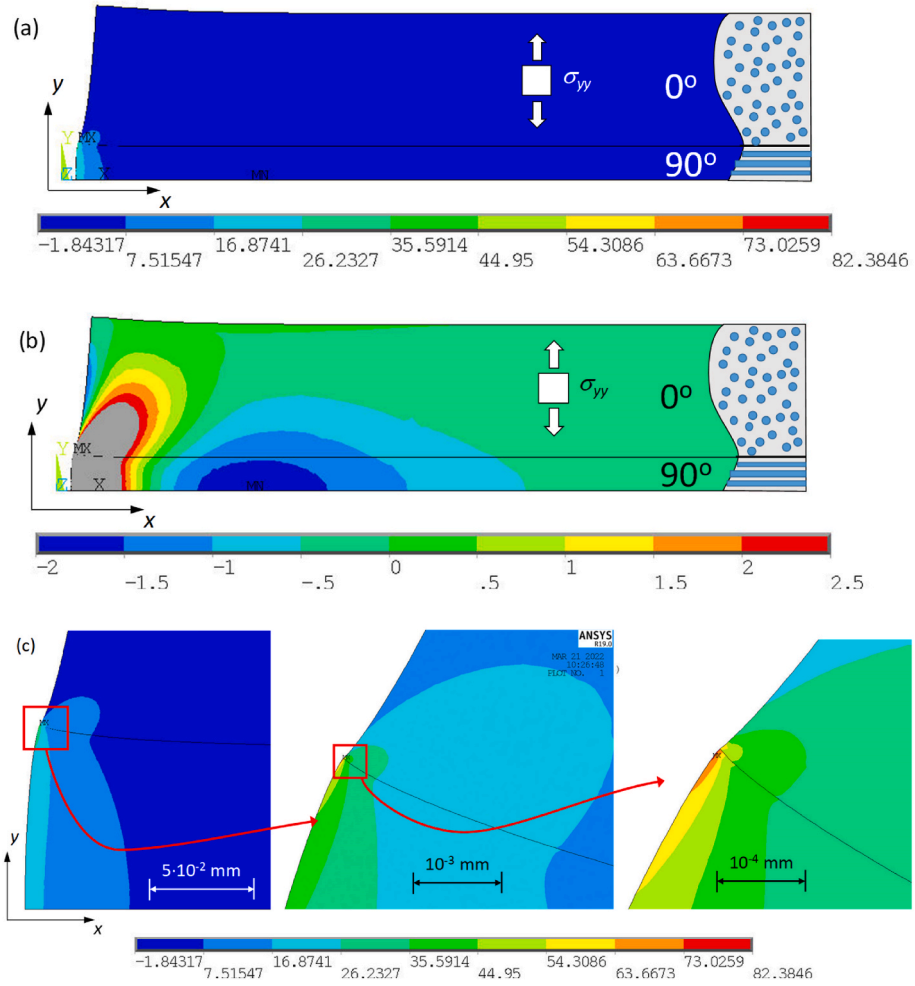

Fig. 3. σ_{yy} contour plots, in MPa, for (a) the whole problem domain, (b) the whole problem domain with selected σ_{yy} contour values, (c) details, at different scales, at the bimaterial corner between 0° and 90° plies.

detailed in a previous work of the authors [26].

Fig. 3 shows, as an example, the σ_{yy} component (in MPa) for the cross-ply laminate under axial extension $u_z > 0$ (values corresponding to a longitudinal $\varepsilon_{zz} = 0.645\%$). As mentioned above, due to the existence of three symmetry planes, only a quarter part of the 2D transverse problem (the cross-section of the sample) is modelled, as depicted in Fig. 2c. Hence, only the top 0° layer and half thickness of the 90° layer are included in the analysis. The bottom and right sides of the model have symmetry boundary conditions. Fig. 3a shows the modelled geometry and illustrates that edge-effect only affects a characteristic distance (in the width direction) of the order of the laminate thickness. Fig. 3b shows the same stress component plot, but σ_{yy} contour values range has been conveniently chosen to clearly see how the presence of tensions at the free-edge, generates slight compression values inside the sample, to fulfil global equilibrium in the vertical direction. The role of these σ_{yy} tensile stresses at the edge will be analyzed later as the responsible for longitudinal cracking in the 90° layer. Finally, Fig. 3c illustrates (by means of three different model magnifications) a more local stress alteration, in the neighbourhood of the bimaterial corner, where assuming linear elasticity, unbounded stresses appear (stress singularity). Results in Fig. 3c have been obtained with a mesh refinement towards the bimaterial corner tip, where the smallest element size is 10^{-6} mm long.

The edge effect and the stress singularity are phenomena which necessarily appear together, each one of them having a different influence (in terms of characteristic length) on the stress field. As can be clearly observed in Fig. 3c, the stress field (in the left-hand side of Fig. 3c) shows an alteration (edge-effect) all along the thickness length at the free edge, whereas the stress field associated with the bimaterial corner singularity (in the right-hand side of Fig. 3c) corresponds to a more local stress alteration, only in the neighbourhood of the bimaterial corner. Due to the intrinsic difficulty in analysing the stress singularity field, it will be studied in a separate section.

3. Stress singularity of the 0/90 bimaterial corner

As mentioned previously in Section 2, stresses are unbounded at those points where material properties, geometry, and/or boundary conditions change abruptly. Obviously, unbounded stresses do not take place in a real specimen, and these stress singularities arise under the assumption of a linear elastic behaviour. Nevertheless, it is widely accepted that the singularity stress representation (in terms of Generalized Stress Intensity Factors and the order of stress singularities) are useful to predict failure initiation or propagation, based on generalized fracture toughness values instead of strength values.

Considering a polar coordinate system (r,θ) at the bimaterial corner, and assuming variable separation, the singularity stress field in the neighbourhood of the corner takes the following form of asymptotic series (for $r \to 0$) (see [17,18] for further information):

$$\sigma_{ij}(r,\theta) = \sum_k K_k r^{-\delta_k} f_{ij}^{(k)}(\theta) \tag{1}$$

where K_k is the Generalized Stress Intensity Factor of mode k, δ_k is the corresponding order of stress singularity ($0 < \mathrm{Re}[\delta_k] < 1$) and $f_{ij}^{(k)}(\theta)$ is the corresponding characteristic angular shape function.

As will be seen later on, the stress singularity in the bimaterial corner, at the intersection of the interface between 0° and 90° layers and the free edge, has only one singular term in the stress representation (1), with $\delta_k < 0.5$, representing a weak singularity. This term affects the characteristic distance where the singularity stress field acts. However due to the fact that the thickness of the ultra-thin plies is very low, it is necessary to try to elucidate whether the singularity affects the whole 90° layer thickness.

Slight geometrical changes at the corner tip, which consist in the modification of the solid wedge angle, allow the stress singularity to be removed, as already done in previous works by the authors (Barroso et al. [6,15]). The same strategy of singularity removal has been carried out in the present work, in order to separate both effects (edge effect and stress singularity) and to check the influence of each one in the zone of interest. The results of such stress singularity removal will be detailed at the end of this section.

Moriya & Ichikawa [16] already proposed slight geometrical modifications of the ply solid angles at the free edge, to remove (or to reduce) the stress singularities appearing at the bimaterial corners between plies at the free-edge of the samples. With straight edges at the lateral faces, solid wedge angles for each material are equal to 90°. The authors in Ref. [16] modified these wedge angles and evaluated the stress singularities for different material systems (high modulus graphite/epoxy, typical graphite/epoxy and typical glass/polyester). The orders of stress singularities (assuming singularities of the power type r^{δ}, with $-1 < \mathrm{Re}[\delta] < 0$) were calculated in Ref. [16] assuming a 2D generalized plane strain state, with stress-free faces and perfect bonding between both materials.

For checking purposes, the authors of the present work carried out the singularity analysis of the problem considered in Ref. [16], and have obtained the same results as those published in (Tables 2, 3 and 4 of Ref. [16]), by using their own semi-analytical procedure (Barroso et al. [17], and Mantič et al. [18]), which was developed for generalized plane strain problems (with $\varepsilon_{zz} = 0$). Nevertheless, the actual problem has $\varepsilon_{zz} \neq 0$, and the equivalence, in terms of singularity results, with the $\varepsilon_{zz} = 0$ problem is not straightforward.

The tool developed by the authors [17,18] is based on the powerful Stroh formalism [25] of anisotropic elasticity assuming generalized plane strain problems with $u_i = u_i(x_1, x_2)$ $(i = 1, 2, 3)$. Stress singularities are obtained semianalytically as the roots of a characteristic equation which depends on the material properties, local geometry, and local boundary conditions of the corner configuration. The whole procedure is analytic except the search of roots of the characteristic equation, which is carried out numerically. Real and complex orders of stress singularities can be obtained. Only stress singularity orders (δ) in a power type structure r^{δ} can be taken into account in the code developed.

To understand this issue, the problem will be separated into two simpler problems, using Eshelby's imaginary cut, deform and bond again procedure [19]. Let us move from the original problem of two bonded layers subjected to an axial extension $\varepsilon_{zz} > 0$ (Fig. 4a), to an alternative problem with each material isolated, no bonding between them (Fig. 4b). If we apply the prescribed $\varepsilon_{zz} > 0$ to both materials, both will elongate the same in the z-direction, but with different σ_{zz} values (Fig. 4c), according to the differences in their Young moduli in this direction (E_{11} for the 0° layer, and E_{22} for the 90° layer). Due to the different values of the Poisson ratio for each ply, the transverse contraction ($\varepsilon_{xx} < 0$) will also be different for each layer (Fig. 4c), higher for the 0° layer and much lower for the 90° layer, due to the fibre orientation in the 90° layer (parallel to the x-direction).

Let us now apply a uniform tensile loading, only to the 0° layer, in the x-direction σ_{xx} (Fig. 4d), but now, under plane strain conditions ($\varepsilon_{zz} = 0$) which implies that the length in the z-direction does not change for this layer, and the corresponding ε_{zz} component which should have appeared due to σ_{xx} (and consequently, ε_{xx}) is zero. This generates an additional σ_{zz} component (only in the loaded 0° layer) associated with the plane strain solution of the problem. The value of the applied σ_{xx} is the necessary one to make the final length of the 0° ply, in the x-direction, to be equal to the length of the already deformed 90° layer in the same direction (Fig. 4e). In this situation, where both lengths (in the x-direction) are the same, we can bond again the materials, without any additional stress needed (Fig. 4f).

At this point (Fig. 4f), stresses in both materials are uniform in the whole volume of each layer:

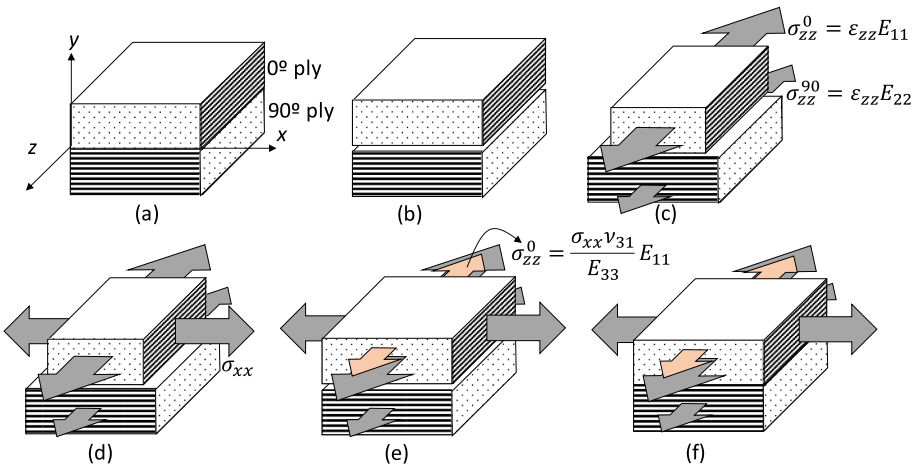

Fig. 4. Decomposition of the original problem.

$$\sigma^0_{ij} = \begin{pmatrix} \sigma_{xx} & 0 & 0 \\ 0 & 0 & 0 \\ 0 & 0 & \sigma^0_{zz}(\varepsilon_{zz}) + \sigma^0_{zz}(\sigma_{xx}) \end{pmatrix}, \qquad \sigma^{90}_{ij} = \begin{pmatrix} 0 & 0 & 0 \\ 0 & 0 & 0 \\ 0 & 0 & \sigma^{90}_{zz}(\varepsilon_{zz}) \end{pmatrix} \tag{2}$$

where: $\sigma^0_{zz}(\varepsilon_{zz}) = \varepsilon_{zz}E_{11}$ is the stress generated in the 0° layer by the global ε_{zz} and the longitudinal stiffness of the material E_{11}, $\sigma^0_{zz}(\sigma_{xx}) = \varepsilon_{zz}(\sigma_{xx})E_{11} = \frac{\sigma_{xx}\nu_{31}}{E_{33}}E_{11}$ is the stress generated, in the plane strain problem, associated with the $\sigma_{xx} > 0 \implies \varepsilon_{xx} = \frac{\sigma_{xx}}{E_{33}} \Rightarrow \varepsilon_{zz} = \varepsilon_{xx}\nu_{31}$ in the 0° ply with the longitudinal stiffness of the 0° ply E_{11} (the fibre orientation being parallel to the z-axis), and $\sigma^{90}_{zz}(\varepsilon_{zz}) = \varepsilon_{zz}E_{22}$ is the stress generated at the 90° ply by the global ε_{zz} with the transverse stiffness of the material E_{22}.

The problem depicted in Fig. 4f (repeated in Fig. 5a) is similar to the one under analysis, with a prescribed $\varepsilon_{zz} > 0$ in both materials, except that there is an additional uniform stress σ_{xx} applied at the lateral faces of the 0° layer. Let us remember that the stress solution to this problem is uniform in both materials. Now, if we just add to this problem (Fig. 5a), with a known uniform stress solution, another problem with the same geometry, with the materials being bonded together, and with a compression σ_{xx} in the same lateral faces of the 0° layer (Fig. 5b), assuming $\varepsilon_{zz} = 0$, the resulting problem would be the desired one under analysis.

It is important to notice that, at the stage illustrated in Fig. 4c, there exists more than one alternative to fulfil the interface displacement compatibility of both solids. For example, instead of applying a $\sigma_{xx} > 0$ in the 0° layer, it is also possible to apply a $\sigma_{xx} < 0$ in the 90° layer, or a particular σ_{yy} compression at the top surface of the 0° ply and at the bottom surface of the 90° ply. In this last alternative, the different Poisson ratio ν_{xy} in both materials would generate different ε_{xx} values, much lower in the 90° layer, as the fibre is oriented in the x-direction. For these three particular solutions there is a value of the applied stress which makes compatible the displacements on both plies along the common interface of the plies.

These alternative ways of facing the original problem also show two important ideas.

- The first, and most important, is that the real problem (with $\varepsilon_{zz} > 0$) has the same solution, in term of stress singularities, as the additional problem (Fig. 5b), assuming $\varepsilon_{zz} = 0$, based on the evidence that the real problem is the superposition of a problem without stress singularities (σ_{ij} is uniform in each ply) (Fig. 5a) and another one which is solved in plane strain, $\varepsilon_{zz} = 0$ (Fig. 5b).
- The second idea is that, although both problems (real and alternative) are equivalent in terms of stress singularities, but the alternative one giving rise to a problem with no stress-free lateral faces (Fig. 5b–c), this issue is associated with the selection of a particular solution of the problem. Let us remind that there is, one alternative particular solution to guarantee the displacements compatibility of both plies along the common interface, mentioned above (applying a $\sigma_{yy} < 0$) which does not introduce loaded lateral faces in the corner problem. Then, the assumption of stress-free lateral faces made in Ref. [16] does not violate the equivalence, and stress singularities calculated assuming ($\varepsilon_{zz} = 0$) are the same than in the real (with $\varepsilon_{zz} > 0$) and alternative (with $\varepsilon_{zz} = 0$) problems.

It is also important to notice that the situation is completely analogous if, instead of prescribing a $\varepsilon_{zz} > 0$ to both materials, we apply a

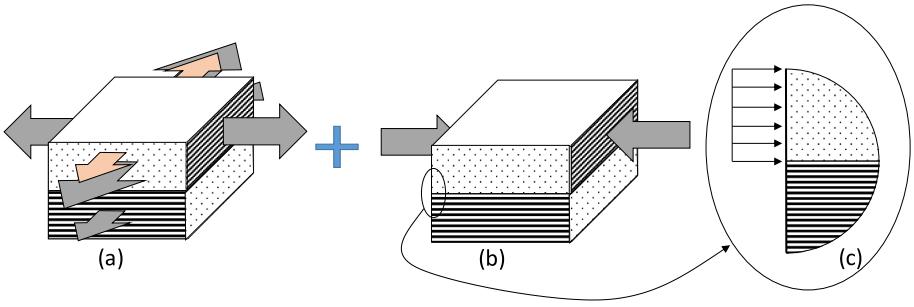

Fig. 5. Superposition of the (a) alternative problem with a uniform stress solution, (b) additional problem (with $\varepsilon_{zz} = 0$) to get the original configuration, and (c) detail of the loaded bimaterial corner.

temperature decrement to both materials. The differences in the thermal expansion coefficients, parallel and perpendicular to the fibre direction respectively, will generate different elongations between both plies, in the *x*-direction, as previously shown in Fig. 4c under mechanical loadings.

Notice also that results in Ref. [16] were obtained under the assumption of a power law r^{δ} for the stress singularity field. This assumption does not agree with the necessary presence of a logarithmic term in the singular stress field predicted by Zwiers et al. [20] for some particular cases of the problem under analysis. Following the results in Ref. [20], the original corner configuration, with two solid wedges of 90° (one for the 0° layer and the other one for the 90° layer) does not need the logarithmic term for the correct asymptotic stress representation, and the stress singularity order δ in a power type structure r^{δ} has been proven to coincide between the numerical model and the semi-analytical tool developed by the present authors [17]. Nevertheless, corners configurations with solid wedge angles different from 90° (in any of the two layers) do not fulfil the condition to have just an r^{δ} term, the presence of an additional ln(*r*) term being necessary.

For the problem under analysis, a finite element model (similar to that used in Fig. 3 but including a notch at the bimaterial corner) has been prepared, with a mesh refinement towards the bimaterial corner tip, with the smallest element size of 10^{-6} mm. The solid angle α of the 0° layer has been progressively reduced (from the starting value of 90°) using a circular notch in the 0° layer, containing the corner tip. The σ_{yy} stress component is plotted along the interface between both plies (Fig. 6), in which the *x*-axis is in the logarithmic scale. The results indicate that for a solid angle of $\alpha \approx 55°$ the stress singularity vanishes (the slope of the stress representation is horizontal). The notch slightly modifies the geometry of the problem (see detail in Fig. 6) but allows to isolate the edge effect and to quantify it separately from the singular stress source. In fact, the different results in Fig. 6 seems to indicate that the extent of the singular stress field (the length that is affected by the presence of the singularity) is below 10^{-2} mm, one sixth of the lowest thickness of the thinnest layer under analysis, which is 0.06 mm (for the 30 g/m^2 ply).

Once the influence (characteristic distance) of the stress singularity has been obtained, in the next section, numerical analyses will be carried out without the presence of the notch, to avoid in the stress field, the "pollution" of the geometrical modification. Obviously, results in the close neighbourhood of the corner vertex will be not taken into account for discussions. The relatively low value of the order of stress singularity (weak singularity) makes the influence of the singularity stress field to be low enough.

4. Numerical results

Two aspects are investigated in this section: the edge-effect associated with the mechanical loading, and the edge-effect associated with the thermal expansion coefficient mismatch. As previously mentioned, the former one is due to the differences in the Poisson ratio of both plies when subjected to a same longitudinal strain ($\varepsilon_{zz} > 0$), whereas the latter

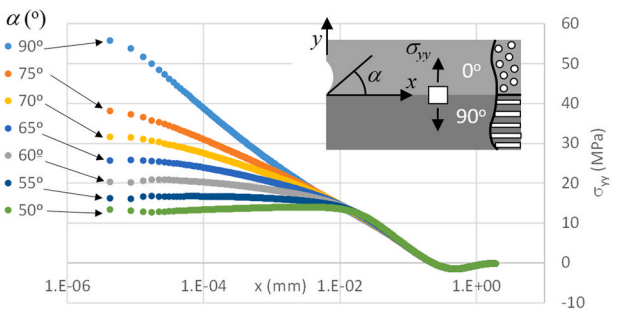

Fig. 6. Stress singularity removal at the bimaterial corner.

corresponds to different values of the thermal expansion coefficients (in the *x*-direction) when subjected to the same temperature decrement (cooling stage in the curing cycle).

Both effects have been analyzed separately because, while the mechanical effect is a direct consequence of the Poisson's ratio values, the thermal effect offers, at least, more uncertainties about the real values of the residual stresses developed in this cooling stage. There are several factors that may affect the full development of a thermal stress field associated with a nominal temperature decrement and a thermal expansion coefficient mismatch. Viscoelastic behaviour can take place in the first stage of the cooling period and stress relaxation can also take place (with time), as clearly shown by the authors, for the materials under study, as will be seen later on. See also [21,22] for other aspects influencing the potential residual stress field due to temperature.

Mechanical properties and thermal expansion coefficients have been experimentally obtained for all materials by the authors (see, for example, Sanchez-Carmona et al. [23] with thermo-mechanical characterization of 30 g/m^2 and 150 g/m^2 plies). Due to the low differences of the mechanical properties obtained for the different materials, and with the aim of avoiding influences other than the role of the thickness itself, average values have been used for the present analyses. These properties, in orthotropic axes, are summarized in Table 1, where "1" is the fibre direction. Y_t is the transverse strength of the material, which is of major importance in the longitudinal failure under analysis. It is important to notice that all numerical models consider all plies as equivalent orthotropic homogenous materials. The adequacy of considering the 90 ply as a heterogeneous or homogeneous material, depend on the object of the study, and in the present case, no particular interest is focused on any micromechanical aspect (at the level of fiber and matrix) of the failure. Nevertheless, only average values across the thickness having been used for reasoning and predictions, no stress-at-a-point has been used for these purposes. Also, for comparison purposes, all numerical models have been analyzed under this assumption.

Notice that the obtained value for α_1 is unusually large, in comparison with other long unidirectional carbon fiber materials. The Coefficient of Thermal Expansion in the fiber direction (α_1) is usually negative for long unidirectional carbon fiber materials, but the values are typically one order of magnitude lower than the values in the transversal directions (α_2, α_3). As (α_1, α_2, α_3) have been obtained in a single test, and (α_2, α_3) are typical values, the authors have consistently decided to trust also on the obtained value for (α_1).

The numerical models are extremely simple in regard to geometry, equal to those in Fig. 3, and only changing the thickness of the 90° layer (30 g/m^2, 50 g/m^2, 100 g/m^2 and 3 × 150 g/m^2). An adequate care has been taken into account to make a good progressive mesh refinement towards the bimaterial corner tip in order to avoid numerical errors which might affect the results far from the corner.

For both numerical models, ANSYS® software has been used, with a 2D geometry (element type PLANE 182) using the Generalized Plane Strain option for this element type.

For the mechanical problem, ANSYS® allows a longitudinal displacement (u_z) (perpendicular to the *x*-*y* 2D geometry) to be introduced in the analysis. Due to the double symmetry of the model, only a quarter of the real geometry has been modelled. In relation with this decision, it is important (not fully detailed in the software help manual) to introduce the longitudinal displacement in the elastic center of the problem (where tensile force and bending moments are uncoupled), in order to apply only tension and not bending moments. Due to the fact that the stiffness of the 0° layer in the *z*-direction (fibre direction) is much higher than the stiffness of the 90° layer in the *z*-direction, a constant ε_{zz} applied to the sample makes the force resultant to be much closer to the center of the 0° layer than to the center of the complete problem (0° and 90°). This elastic center has been calculated and results of the 2D model have been verified using a 3D model with the complete geometry of the sample (no symmetries applied).

Table 1
Thermo-mechanical properties of the materials.

E_{11}(GPa)	E_{22}(GPa)	E_{33}(GPa)	G_{12}(GPa)	G_{13}(GPa)	G_{23}(GPa)	ν_{12}	ν_{13}	ν_{23}
113.91	7.81	7.81	3.25	3.25	2.35	0.32	0.32	0.40
Yt (MPa)		α_1 (°C^{-1})			α_2 (°C^{-1})			α_3 (°C^{-1})
38		$-1.37{\cdot}10^{-5}$			$1.74{\cdot}10^{-5}$			$1.70{\cdot}10^{-5}$

For the mechanical analysis, a displacement (u_z) giving rise to a longitudinal strain $\varepsilon_{zz} = 0.003871$ has been applied. This ε_{zz} generates a nominal $\sigma_{zz} = \varepsilon_{zz}{\cdot}E_{22} = 30$ MPa in the 90° layer, which is close to the experimentally obtained transverse strength of the material ($Y_t = 38$ MPa). All these values, predicted by the Classical Lamination Theory, have been verified in the numerical model, in areas far away from the free-edge.

As the main numerical result for the present work, Fig. 7 shows the σ_{yy} stress component, in the 90° ply, along the free edge ($x = 0$) of the sample. Horizontal axis represents the ratio between the y coordinate and half of the 90° layer thickness of the model. Taking into account that only a quarter of the real problem is modelled, y/thickness = 0 corresponds to the center of the 90° ply, whereas y/thickness = 1 corresponds to the upper part of the 90° ply, in contact with the 0° ply. This dimensionless parameter allows different models with different 90° thicknesses to be compared, which is the main objective of the present work. Two vertical axes have been used in Fig. 7, the left-hand side axis shows the ratio between the σ_{yy} stress component and the transverse strength of the material (Y_t), while the right-hand side axis shows the ratio between σ_{yy} and the applied longitudinal stress σ_{zz}. Due to the fact that the transverse strength is $Y_t = 38$ MPa and the applied longitudinal stress is $\sigma_{zz} = 30$ MPa, both axes are slightly different. The text "MECH" in the legend, refers to "MECHanical loading".

In Fig. 7, four thicknesses (0.485 mm, 0.1 mm, 0.065 mm and 0.06 mm), associated with the four laminates under analysis (450, 100, 50 and 30) have been numerically studied. Let us remember that the results near the bimaterial corner vertex cannot be taken into account, due to the presence of the weak singularity. Far from the characteristic distance of the singularity field influence (for example, in the range 0 < y/thickness<0.8) results are exclusively due to the edge-effect and are not affected by the stress singularity. Recall that Classical Lamination Theory predicts $\sigma_{yy} = 0$, and this result is valid as long as we go far away from the free-edge (see Fig. 3a–b).

It is worth highlighting, from results in Fig. 7, that the thinner the 90° layer the higher the σ_{yy} stresses along the free edge. For conventional 90° layer thicknesses (for example 450 g/m^2) σ_{yy} keeps below 50% of the longitudinal applied (σ_{zz}) stress, but for ultra-thin plies in the 90° layer (for example 30 g/m^2 or 50 g/m^2) σ_{yy} moves in the range between $0.6\ \sigma_{zz} < \sigma_{yy} < 0.8\ \sigma_{zz}$.

These values of σ_{yy} are not high enough by themselves, to make longitudinal cracks to appear before the transverse cracks, associated with σ_{zz}, but it should be also taken into account the contribution of the residual thermal stresses originated by the cooling stage of the curing cycle.

Fig. 8 shows the same stress component along the same free edge, but now associated with the thermal effect. From the curing temperature (135 °C) to room temperature (25 °C) the bonded laminate suffers a $\Delta T = -110$ °C. Although, as mentioned previously, some stress relaxations might appear with time, let us take the results in Fig. 8 as an upper limit of the thermal residual stresses in the present problem. As in the mechanical case, σ_{yy} (due to ΔT) gets negligible values far away from the free-edge, but at the free-edge, numerical results predict, with the exception of the 450 g/m^2 material, σ_{yy} values higher than the transverse strength (Y_t) of the material, between $1.7\ Y_t < \sigma_{yy} < 2.0\ Y_t$ for the whole 90° layer thickness. The text "TEMP" in the legend, refers to "TEMPerature" loading.

These stresses should be added to those originated by the mechanical effect, and although some stress relaxation might appear, in the thinnest laminates (30 g/m^2 and 50 g/m^2) only the thermal stresses (or the sum of thermal and mechanical contributions in some cases) are high enough to make the longitudinal cracks to appear before transverse cracks, as experimentally observed, even before the mechanical loading is applied.

The clear influence that the ply thickness has on the σ_{yy} stress values along the free edge might be explained by using Eshelby's imaginary cut, deform and bond again procedure, previously introduced in Fig. 4. Recall that, to fulfill compatibility with the 0° layer, the 90° layer is subjected to a prescribed displacement in the x-direction (applied along its top surface). This prescribed displacement is independent of the 90° layer thickness, thus, generating higher shear strains (and consequently the local strain and stress alteration) as the 90° layer thickness

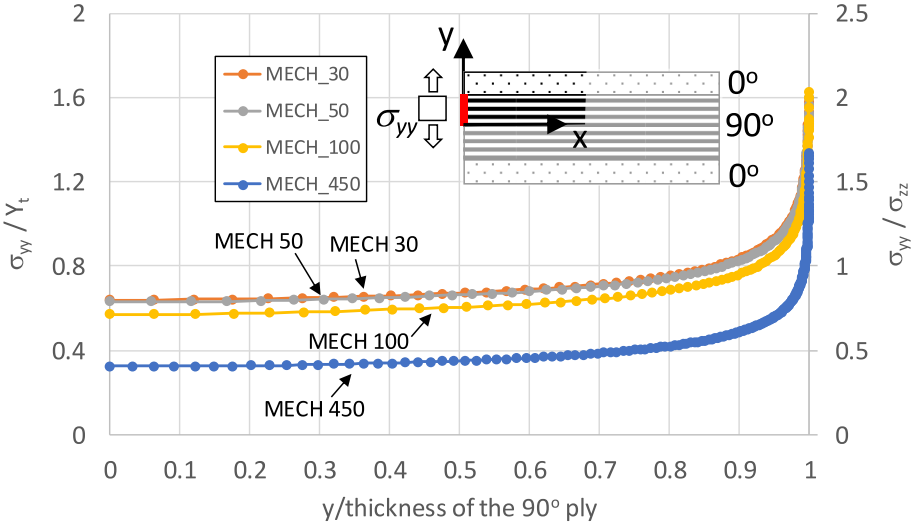

Fig. 7. σ_{yy} stress component along the free-edge, due to a mechanical loading (σ_{zz}).

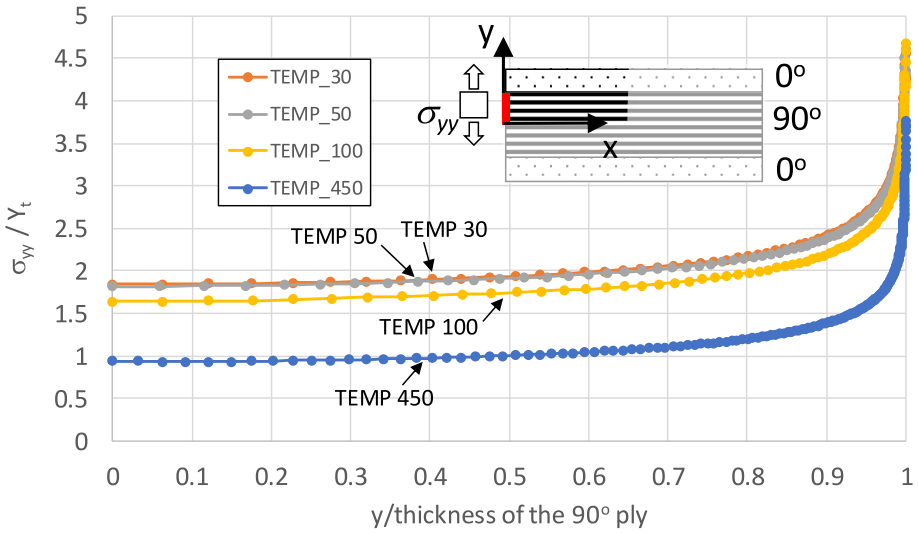

Fig. 8. σ_{yy} stress component along the free-edge, due to the thermal effect ($\Delta T = -110$ °C).

decreases.

In order to support more evidence of the stress relaxation associated with the thermal effect for these materials, non-symmetric $[0_4/90_4]$ laminates have been manufactured with 30 g/m^2 and 100 g/m^2 prepregs [1]. These laminates show a curvature after the curing cycle (curing temperature 135 °C), which changes with time. Fig. 9 shows the radius of curvature measured from instants after the curing cycle, to more than 1000 h later. The increment of the radius of curvature of the laminate with time R(t), in a laboratory temperature and relative humidity controlled ambient, and no external load applied, is a clear indication of the previously mentioned stress relaxation (at room temperature).

Numerical (Finite Element) simulations, taking into account only the thermal effect derived from the cooling down stage after the curing process in the present laminates (no chemical shrinkage, or any other source of residual stresses), show that thermal stresses (after 1000 h) are between 50% and 60% of those generated by the nominal temperature decrement between curing and room temperatures, $\Delta T = -110$ °C. These values, by themselves, or added to those generated by the mechanical loadings, can still reach values close to the strength (Y_t) of the material.

As a complementary result, Fig. 10 shows the alteration of the σ_{zz} stress component at the free-edge, both due to the mechanical loading (Fig. 10a) as well as the thermal loading (Fig. 10b). Similarly, as done in Figs. 7 and 8 (with σ_{yy}), the stress values in the vertical axis are plotted with respect to the nominal applied σ_{zz}, in the case of the mechanical load (Fig. 10a), and also with respect to Y_t (Fig. 10a and b). This stress component does not have a direct responsibility in the longitudinal failures under analysis (if we assume that failure is governed by a maximum stress criterion), but it is clear, from Fig. 10a and b that, at the free-edge, the longitudinal σ_{zz} values are higher than the nominal σ_{zz} value generated as a result of the applied ε_{zz}.

5. Failure inspection by 3D X-ray imaging

Once the sources of the normal stresses in the thickness direction of the sample have been identified and quantified, it is of major importance to check if this failure had progressed along the width of the sample, or it was limited to the free-edge vicinity. Let us remember (Fig. 3b) that the tensile normal stresses σ_{yy} appear along distance of one or two laminate thicknesses in the width direction, from the free edge, this stress component being slightly in compression ($\sigma_{yy} < 0$), to guarantee global equilibrium in the *y*-direction. Therefore, if the onset of failure is due to the edge-effect, its influence should be limited to a characteristic distance in the width direction.

Inspection of some longitudinal failures were carried out using a non-destructive 3D Computed Tomography (ZEISS® Xradia 620 Versa). The inspection was carried out near the low limit level of the equipment, with a pixel size of 0.3336 μm, 4501 projections in a 180° inspection range, source settings were 50 kV and 90 μA. 3D reconstructions were done with Dragonfly Pro® software.

It is worth remembering that, with a fibre diameter of 6–7 μm, the maximum opening of the lips of the longitudinal fibre-matrix interface crack are below 1–2 μm. As the crack grows in the width direction,

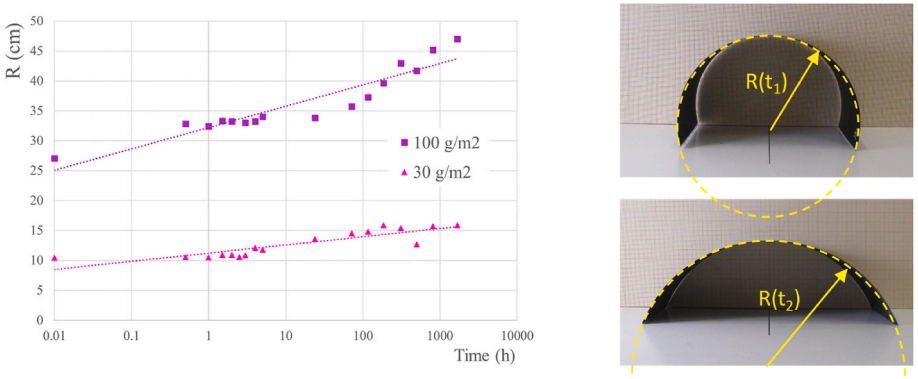

Fig. 9. Stress relaxation in non-symmetric $[0_4/90_4]$ 30 g/m^2 and 100 g/m^2 laminates.

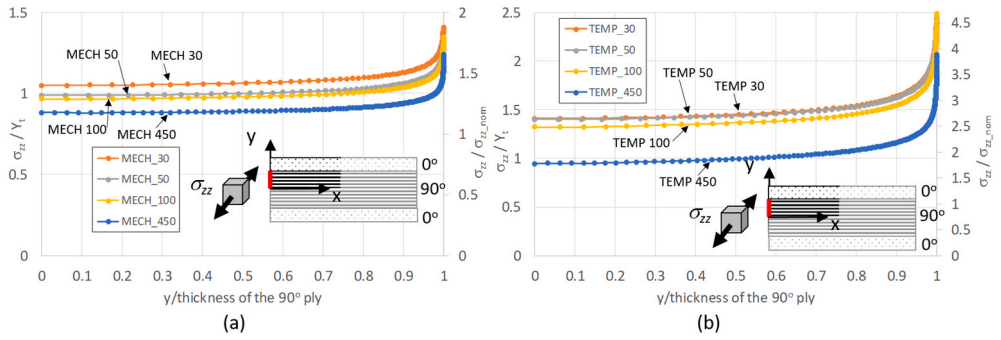

Fig. 10. σ_{zz} stress component along the free-edge, due to a) mechanical loading, b) thermal effect ($\Delta T = -110$ °C).

opening values are much lower and, in some cases, the crack length measurement might be a lower limit of the real crack length, due to the impossibility of the equipment to detect the crack opening.

It is also noticeable that, while in glass fibre laminates, failures can be observed with the use of a back light source, this solution is not possible in the case of carbon fibre laminates, the adopted solution being one of the few possibilities to make this inspection.

Some samples having longitudinal failures after the curing cycle were polished in the lateral face to identify (by optical microscopy) the location of the failure. It is important to notice that the lateral sanding and polishing of the sample removes approximately 1 mm of the sample material in the width direction, but it is mandatory for a good location of the damage before tomographic inspection.

Some examples of 3D computed tomography reconstructions are shown in Fig. 11.

- Fig. 11a is a lateral view of the sample, where 0° plies can be seen at both sides of the 90° ply (in the middle), with the longitudinal (vertical) failure (in yellow).
- Fig. 11b shows an oblique perspective of the same failure, highlighting the longitudinal failure in a colors scale which identifies the opening distance of the two faces of the longitudinal crack.
- Fig. 11c is exactly the same previous image but eliminating the laminate.
- Fig. 11d is the zenithal view of the sample, which allows the crack length in the width direction (horizontal direction) to be measured. The left-hand side of the image is the sanded surface of the lateral side of the sample.

The polishing of the lateral surface, removing almost 1 mm from the lateral side of the sample is necessary, as mentioned above, to precisely locate the longitudinal crack for the detailed inspection, but it avoids having a picture of the real edge failure extension. In Fig. 11d, after eliminating approximately 1 mm from the free edge, it was still possible to measure longitudinal failures penetrating only 85 μm, in the width direction, from the free edge.

What it is important is that these experimental observations indicate that the observed failure does not progress along the whole width of the sample, 25 mm, (no tunneling) and clearly support that the failures are a result of the edge effect.

Due to its inherent complexity, a detailed analysis of the progression of these longitudinal failures along the width of the sample, under fatigue loading, falls out of the scope of this paper. The influence of the failure progression along the width on the stiffness degradation (mainly in bending) is currently being investigated.

6. Conclusions

Non-conventional failures in cross-ply laminates with ultra-thin plies have been identified and a plausible explanation of their causes has been given by means of the edge effect. These non-conventional failures consist in longitudinal cracks/debonds (parallel to the loading direction) in the 90° ply. The most important aspects of the present work are summarized below.

- The observed non-conventional failures increase as the 90° layer thickness decreases. The use of ultra-thin plies in the present work defines a clear difference with previous published works. Conventional transverse damage decreased with the same trend.
- Stress singularity at the corner between the 0° and 90° interface with the free-edge has been characterized. Due to the extremely low values of the 90° layer thickness, it is important to check the characteristic distance of the singularity stress influence. In the present work, slight geometric changes have been proposed in the corner to remove the singularity, isolating the influence of both effects (singularity and edge-effect).
- Numerical analyses, under mechanical loading as well as under thermal loading, have been carried out to evaluate the alteration of the stress field at the free edge. Some experiments have been also

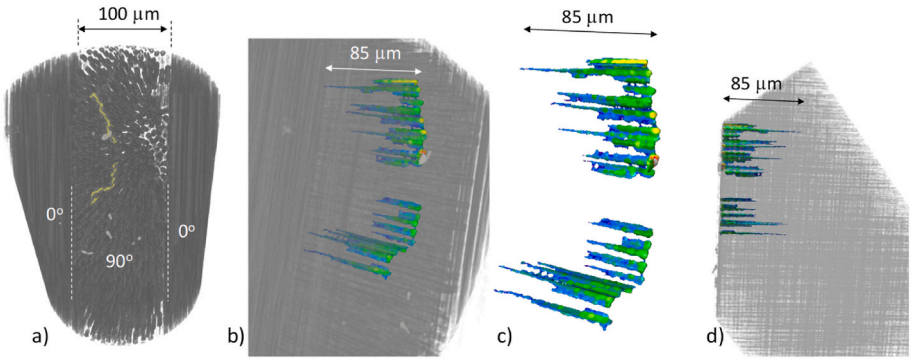

Fig. 11. 3D reconstructions of the longitudinal failure inspection.

carried out to assess the relaxation with time of the residual thermal stresses for the materials under analysis.

- Stresses originated by the edge effect due to the mechanical loading have shown to be close to the 70% of the longitudinal applied stress. For the thermal loading, stresses originated at the free edge are above the transverse strength of the material (Y_t) for the nominal temperature decrement between curing and room temperatures.
- 3D computed tomography was used at submicron level to evidence that failures under analysis have not crossed the whole width of the samples, but are limited to the close vicinity of the free edge of the samples.

CRediT authorship contribution statement

Sánchez-Carmona S: Conceptualization, Experimental methodology, Writing – review & editing. Barroso A: Conceptualization, Investigation, Computational Methodology, Writing – original draft, Funding acquisition. Mantič V: Conceptualization. Investigation, Writing – review & editing, Funding acquisition. Correa E: Conceptualization. Investigation, Writing – review & editing, Funding acquisition. París F: Supervision, Writing - review & editing.

Declaration of competing interest

The authors declare the following financial interests/personal relationships which may be considered as potential competing interests: Barroso A reports financial support was provided by Government of Andalusia Ministry of Economic Transformation Industry Knowledge and Universities. Mantic V reports financial support was provided by Spain Ministry of Science and Innovation. Correa E reports was provided by Spain Ministry of Science and Innovation.

Data availability

Data will be made available on request.

Acknowledgements

The research was conducted with the support of Spanish Ministry of Science, Innovation and Universities, Projects PID2021-126279OB-I00 and PID2021-123325OB-I00, Consejería de Transformación Económica, Industria, Conocimiento y Universidades, Junta de Andalucía and the European Regional Development Fund: P18-FR-1928 and P18-FR-3360; and the Universidad de Sevilla: grant VIPPIT-2018-II.2.

The authors also acknowledge the valuable help of Agustín Cota and Simona Scrivano, Specialist Technicians from the X-Ray department at CITIUS, and the students Ester Culebras and Jorge Marín.

References

[1] Sánchez-Carmona S, Correa E, Barroso A, París F. Experimental observations of fatigue damage mechanisms in cross-ply laminates using carbon-epoxy ultra-thin plies. Compos Struct 2023;306:116564.
[2] Parvizi A, Garret KV, Bailey JE. Constrained cracking in glass fibre-reinforced epoxy cross-ply laminates. J Math Sci 1978;13:195–201.
[3] Flaggs DL, Kural MH. Experimental determination of the in situ transverse lamina strength in graphite/epoxy laminates. J Compos Mater 1982;16:103–16.
[4] García IG, Justo J, Simon A, Mantič V. Experimental study of the size effect on transverse cracking in cross-ply laminates and comparison with the main theoretical models. Mech Mater 2019;128:24–37.
[5] París F, Velasco ML, Correa E. The scale effect in composites: an explanation physically based on the different mechanisms of damage involved in failure. Compos Struct 2021;257:113089.
[6] Barroso A, Marín JC, Mantič V, París F. Premature failures in standard test specimens with composite materials induced by stress singularities in adhesive joints. Int J Adhesion Adhes 2020;97:102478.
[7] Pipes RB, Pagano NJ. Interlaminar stresses in composite laminates under uniform axial extension. J Compos Mater 1970;4:538.
[8] Pagano NJ, Soni SR. Chapter 1 - Models for studying free-edge effects. In: Pagano NJ, editor. Interlaminar response of composite materials, 5; 1989. p. 1–68. Composite Material Series.
[9] Kassapoglou C, Lagace PA. Closed form solutions for the interlaminar stress field in angle-ply and cross-ply laminates. J Compos Mater 1987;21:292–308.
[10] Becker W. Closed-form solution for the free-edge effect in cross-ply laminates. Compos Struct 1993;26:39–45.
[11] Pagano NJ, Schoeppner GA, Kim R, Abrams FL. Steady-state cracking and edge-effects in thermo-mechanical transverse cracking of cross-ply laminates. Compos Sci Technol 1998;58:1811–25.
[12] Lorriot Th, Marion G, Harry A, Wargnier H. Onset of free-edge delamination in composite laminates under tensile loading. Composites Part B 2003;34:459–71.
[13] Mittelstedt C, Becker W. Free-edge effects in composite laminates. ASME Appl. Mech. Rev. 2007;60:217–45.
[14] Mittelstedt C, Becker W, Kappel A, Khargani N. Free-edge effects in composite laminates—a review of recent developments 2005–2020. ASME Appl. Mech. Rev. 2022;74:217–45.
[15] Barroso A, Lauke B, Mantič V, París F. Tensile and shear strength of bimaterial interfaces within composite materials. Compos Sci Technol 2016;124:81–8.
[16] Moriya K, Ichikawa T. A study on edge protection against delamination for composite laminates (The effects of edge shapes on stress singularities for cross-ply laminates). JSME Int J Ser III 1988;31:209–14.
[17] Barroso A, Mantič V, París F. Singularity analysis of anisotropic multimaterial corners. Int J Fract 2003;119:1–23.
[18] Mantič V, Barroso A, París F. Singular elastic solutions in anisotropic multimaterial corners. Applications to composites. In: Mantič V, editor. Mathematical methods and models in composites. Imperial College Press; 2014. p. 425–95.
[19] Eshelby JD. The determination of the elastic field of an ellipsoidal inclusion, and related problems. Proc Roy Soc Lond Math Phys Sci 1957;241:376–96.
[20] Zwiers RI, Ting TCT, Spilker RL. On the logarithmic singularity of free-edge stress in laminated composites under uniform extension. J Appl Mech 1982;49:561–9.
[21] Barroso A, Vicentini D, París F, Mantič V. Representativity of thermal stresses in designing composite joints based on singular stress states at multimaterial corners. Compos Appl Sci Manuf 2011;42:1084–92.
[22] Barroso A, Vicentini D, París F, Mantič V. Thermal stresses in composite joints. In: Hetnarski RB, editor. Encyclopedia of thermal stresses. Springer; 2014. p. 5323–33.
[23] Sánchez-Carmona S, Velasco ML, Barroso A, Correa E. Thermomechanical characterisation data of 30 g/m2 and 150 g/m2 cured unidirectional carbon/epoxy tape prepreg TP 402/T700S. Data in Brief 2023. Accepted for publication.
[24] Neogia A, Mitrab N, Talreja R. Cavitation in epoxies under composite-like stress states. Compos Appl Sci Manuf 2018;106:52–8.
[25] Ting TCT. Anisotropic elasticity: theory and applications. Oxford University Press; 1996.
[26] París F, Velasco ML, Correa E. Micromechanical study on the influence of scale effect in the first stage of damage in composites. Compos Sci Technol 2018;160:1–8.